Solar-Terrestrial Physics. 2025, vol. 11, iss. 4, pp. 120–129. DOI: 10.12737/stp-114202513. © 2025 D.A. Stukov, N.V. Yagova. Published by INFRA-M Academic Publishing House

DOI: 10.12737/stp-114202513

Received April 03, 2025
Accepted August 06, 2025

COHERENCE TIME SCALES OF LONG-PERIOD ULF VARIATIONS OF MAGNETIC FIELD IN VICINITY OF THE NIGHT-SIDE MAGNETOPAUSE

D.A. Stukov
Schmidt Institute of Physics of the Earth RAS, Moscow, Russia, sda@ifz.ru
Institute of Solar-Terrestrial Physics SB RAS, Irkutsk, Russia

N.V. Yagova
Schmidt Institute of Physics of the Earth RAS, Moscow, Russia, nyagova@ifz.ru

Abstract. We examine magnetic field variations within the frequency range of several millihertz (Pc5-6/Pi3 geomagnetic pulsations) in the near-Earth magnetotail and adjacent flank magnetosheath regions, using data from Cluster satellites for 2016. Dependence of spectral coherence on interval length is analyzed for a satellite pair Cluster-1 and Cluster-4 at different satellite positions relative to the magnetopause. It is shown that absolute coherence and the rate of its decline with increasing time interval length differ for the longitudinal and transverse magnetic field components, as well as for different satellite positions. We also present a case study of a coherent pulsation recorded in the magnetosheath at low solar wind velocity and weak fluctuations in front of the bow shock.

Keywords: Pc5-6/Pi3 geomagnetic pulsations, magnetotail, magnetopause, magnetosheath, coherence.

INTRODUCTION

The magnetotail features magnetohydrodynamic (MHD) oscillations of all main types, recorded in the magnetosphere, and its specific flapping modes (see, e.g., the review [Leonovich et al., 2015]). Experimental data confirms that global geomagnetic pulsations can be observed in the magnetotail at distances up to tens of Earth radii (R_E). Wang et al. [2015] have shown that the average amplitude of Pc5 pulsations correlates with fluctuations in the solar wind (SW) dynamic pressure P_{sw}, which is consistent with the role of SW as an external source of excitation of MHD oscillations.

In [Nosikova et al., 2022; Yagova et al., 2022; Yagova, Evsina, 2024], it has been found that the dependence of the pulsation amplitude in the tail on the intensity of fluctuations in the interplanetary magnetic field (IMF) and SW dynamic pressure components in front of the bow shock (we will call such fluctuations “external fluctuations”) differs for pulsations of different spatial scales. Large-scale pulsations are characterized by an almost identical form of variations and a small phase incursion at distances of the order of several R_E. Their amplitude weakly depends on the intensity of external fluctuations, and hence it is these pulsations that dominate at a low level of external disturbance. Under such conditions, the pulsations demonstrate a relatively high quality and a weak relationship with magnetic field fluctuations in the nightside magnetosheath. At a higher level of fluctuation amplitudes in front of the bow shock, the contribution of smaller-scale pulsations, whose amplitude depends greatly on the amplitude of external fluctuations, increases; and the proportion of coherent pulsations grows on both sides of the magnetopause.

The spectral power density and coherence were estimated in [Nosikova et al., 2022; Yagova et al., 2022; Yagova, Evsina, 2024] for a fixed interval length, but the possibility of using the estimates obtained on other time scales was not explored. Meanwhile, the time scale of coherence is an important characteristic of disturbance of a medium. Analysis of time and spatial scales of coherence is widely used for studying turbulence, in particular in the interplanetary medium and magnetosheath. For example, Gutynska et al. [2008, 2009] investigated time scales of coherence with a method based on the analysis of individual wave packets. To do this, correlations between oscillations in the magnetic field modulus were estimated as function of time delay for shifts up to 20 min. From this analysis, Gutynska et al. [2012] draw a conclusion that for frequencies below 10^{-2} Hz oscillations always have a source in front of the bow shock in contrast to higher frequencies that can be excited directly in the magnetosheath.

The most comprehensive statistical study of turbulence spectra in the magnetosheath in the frequency range from millihertz to several hertz has been carried out in [Rakhmanova et al., 2024], which continues the series of studies [Zastenker et al., 2002; Shevyrev et al., 2003, 2007; Rakhmanova et al., 2020] (for more detail, see [Rakhmanova et al., 2023]).

When examining turbulence parameters, it is necessary to cover the widest possible frequency range. Studies on turbulence in the magnetosheath describe spectra of variations in plasma and magnetic field parameters. The main attention in studies of magnetic field fluctuations in the magnetosheath is paid to higher frequencies than the frequencies of long-period pulsations we deal with in this paper. Oscillations with frequencies of several millihertz are either not examined at all or lie on the boundary of the range in question [Gutynska et al., 2009]. The results on long-period variations are not always commented on by authors, and in this frequency

range there is a risk of decreasing accuracy since the lower frequency limit turns out to be on the order of or even less than the inverse length of the interval under study [Alexandrova et al., 2008; Gutynska et al., 2009].

Analysis of spectra and polarization of magnetic field variations in the magnetosheath in the range from a few millihertz to 10 Hz carried out in [Alexandrova et al., 2008] has shown that in most cases the main power is concentrated in the transverse components. The spectra presented by the authors demonstrate spectral maxima in the millihertz spectral region, but the question about properties of quasi-harmonic oscillations in the millihertz range in the magnetosheath is not addressed in the work. Huang et al. [2017] analyze the power spectral density (PSD) and spectral slopes, using Cluster satellite data obtained in the magnetosheath in the frequency range from a few millihertz to tens of hertz. The emphasis is on the change in the spectral slope during the transition from inertial to dissipative mode and on properties of oscillations of the longitudinal field component. The spectra were calculated and the spectral slope was estimated from 1.6 hr intervals, which makes it possible to correctly assess spectral parameters in the range of several millihertz. For individual events analyzed in the paper, there are spectral maxima in the dayside magnetosheath, which are not commented on by the authors.

Stukov and Yagova [2024] have indicated that a decrease in the degree of coherence with increasing interval length T is approximately the same for the tail lobe and the magnetosheath at T~1 hr, whereas at large T values the degree of coherence in the magnetosheath decreases faster than in the geomagnetic tail. This paper continues the analysis of variations in the millihertz range in the magnetotail carried out in [Nosikova et al., 2022; Yagova et al., 2022; Yagova, Evsina, 2024; Stukov, Yagova, 2024]. The time scales of coherence throughout 2016 are studied for the near tail and adjacent flank magnetosheath regions from Cluster-1 and -4 data.

1. DATA AND PROCESSING

The Cluster mission [Escoubet et al., 2001, 2015] includes four satellites. Their instantaneous positions form a tetrahedron that makes it possible to explore 3D distributions of the magnetic field, plasma parameters, and particle fluxes. Orbits of the satellites are highly elliptical with an apogee of ~20 R_E and a perigee of ~4 R_E, sequentially crossing the magnetosheath, the magnetopause, and the magnetotail.

The magnetic field was measured by a fluxgate magnetometer FGM with a time step ~0.045 s. On the website [https://cdaweb.gsfc.nasa.gov/], the data is available in several time resolutions, from initial to several minutes. We have used data for 2016 with a time step ~4 s. Their primary processing involved choosing the position of the satellites from [https://sscweb.gsfc.nasa.gov/], as well as selecting intervals lasting more than 2.5 hrs without gaps and peaks caused by equipment failures.

For the selected continuous data fragments, the transition was made from the geocentric solar-ecliptic coordinate system GSE to the coordinate system associated with the magnetic field. The main magnetic field was determined from the satellite's measurements. For each moment of time t_0, the vector of the main magnetic field $\mathbf{B}_{av}$ was found by averaging in a 20 min running window (t_0±10 min). For the current value of the magnetic field $\mathbf{B}(t_0)$, a transition was performed to a new coordinate system with B_τ, B_ρ, B_ϕ, where B_τ is codirectional with $\mathbf{B}_{av}$; B_ρ is perpendicular to B_τ and lies in the plane formed by $\mathbf{B}_{av}$ and the Earth–satellite line, and B_ϕ closes the right three vectors. The time series thus obtained has the same digitization step as the original one, and allows us to examine variations in the magnetic field relative to the main field, determined from the satellite's measurements, at frequencies higher than the inverse length of the averaging interval.

For further analysis, we took orbital sections when the satellites were located in one of the following regions: tail lobe, high-latitude boundary layer (HLBL), and flank magnetosheath — nightside and dayside magnetosheath away from the subsolar point ($X_{GSE}<3R_E$). Next, we selected time intervals belonging to one of three classes determined from the position of Cluster-1 and -4 relative to the magnetopause: Both IN — both satellites in the tail lobe; Both OUT — both satellites in the magnetosheath; MPCross — the satellites near the magnetopause. The last class includes intervals with instants of time when one satellite is in HLBL; and the other, in the magnetosheath; for all points in the interval, the distance from the magnetopause D_{MP} (based on the model location of the magnetopause according to [https://sscweb.gsfc.nasa.gov/]) satisfies the condition $-2\ R_E<D_{MP}<0.6\ R_E$. For Both IN, $D_{MP}<-2\ R_E$; for Both OUT, $D_{MP}>0.6\ R_E$. Thus, the classes do not touch.

The total number and total length of intervals in each class are listed in Table. We deal with intervals from 48

The number of intervals for each T and their total length ΣT in minutes for three satellite position classes

Interval length T, min	Both IN		Both OUT		MPCross	
	N	ΣT	N	ΣT	N	ΣT
48	**945**	**15888**	**346**	**5904**	**127**	**2352**
64	**897**	**15424**	**322**	**5568**	**109**	**2240**
80	**851**	**14880**	**301**	**5440**	**92**	**1840**
96	**807**	**14400**	**281**	**5184**	**80**	**1920**
112	**764**	**14224**	**261**	**5376**	69	1568
128	**723**	**13696**	**241**	**4736**	61	1536
144	**683**	**13680**	**222**	**4752**	54	1152

to 144 min with a step of 16 min. The minimum interval length for spectral analysis is approximately three full oscillation periods at the lower limit of the frequency range under study, and the maximum one is limited to the time the satellite is located in the region of interest. The sequence of intervals for spectral analysis is selected from continuous data fragments of each class. The step between adjacent intervals is 16 min. The use of the overlap allows edge effects to be avoided. Due to the overlap, the total length of the intervals may be less than the product of the interval length by their number. $\Sigma T=20T$ is taken as the threshold value for further analysis and presentation of the results in plots. The values satisfying this condition are highlighted in bold in Table.

The data was processed in Python with the SciPy library, which ensures the implementation of spectral analysis and time series processing algorithms. Spectral estimation was performed using the following parameters: a Blackman window of width ΔT=16 min (960 s), a segment of length N_{perseg}=32, an overlap $N_{overlap}$ =24, and the number of points for fast Fourier transform N_{fft}=128. For the chosen intervals in the frequency band 1.2÷4.2 mHz, we calculated PSD and spectral coherence $\gamma^2(f)$. PSD was found for three magnetic field components for each satellite; and $\gamma^2(f)$, for all pairwise combinations of b_{c1}—b_{c4}, where the c index takes the values (τ, p, ϕ), and the numeric index corresponds to the Cluster number. To designate variations in the magnetic field components and their spectra, lowercase b is used to distinguish them from the designations of the components of the full field.

2. RESULTS

2.1. Coherence. Statistics

The coherence matrix is symmetric and generally contains six different elements: three diagonal (for components of the same name) and three nondiagonal. Figures 1–3 plot the dependences of the band mean $\langle\gamma^2\rangle$ for longitudinal and transverse magnetic field components when satellites are in tail lobes, in the vicinity of the magnetopause, and in the nightside magnetosheath. Figures 1–3 indicate that for all satellite positions and T values the nondiagonal elements of the coherence matrix are smaller than the diagonal ones; therefore, they are excluded from further analysis.

Figures 4–6 present a more complete set of coherence parameters for diagonal elements. The band mean $\langle\gamma^2\rangle$ and maximum γ^2_{max} are considered. The $\langle\gamma^2\rangle$ and γ^2_{max} values average for each class are given in top panels of Figures 4–6. Bottom panels show the probability of occurrence of over-threshold values $P(\langle\gamma^2\rangle>0.5)$, defined as the ratio of the number of intervals, such that $\langle\gamma^2\rangle>0.5$, to the total number of intervals N, and $P(\gamma^2_{max}>0.75)$, determined similarly for γ^2_{max}. For brevity, the term “coherence” is employed to describe the results common to all coherence parameters.

Figure 4 demonstrates the coherence dependence on T for the longitudinal component b_τ. All coherence parameters decrease with increasing interval length and reveal a qualitatively identical dependence on the position of the satellites. Maximum coherence values for all T correspond to Both IN: $\langle\gamma^2\rangle>0.6$ for all T; at T=48 min it reaches 0.8; $\gamma^2_{max}>0.8$ for all $T<128$ min. The probability of occurrence of over-threshold values for both $\langle\gamma^2\rangle$ and γ^2_{max} exceeds 0.6 for all T. MPCross has the lowest coherence, and for Both OUT the coherence parameters assume intermediate values.

For both parameters describing $\langle\gamma^2\rangle$, the differences between MPCross and Both OUT are small, but they are well-defined for γ^2_{max}. Common to all coherence parameters is that the differences between the classes increase with T. This effect is weaker for interval-average $\langle\gamma^2\rangle$ and is the strongest for $P(\gamma^2_{max}>0.75)$. At T=80 min, $P(\gamma^2_{max}>0.75)$ for MPCross is almost twice as small as that for Both IN, whereas at T=48 min the difference is ~25 %.

Thus, the coherence between the longitudinal components is characterized by maximum values in the tail lobe, minimum values in the vicinity of the magnetopause, and intermediate values in the magnetosheath. The difference increases with interval length and is more pronounced for γ^2_{max} and the probability of occurrence of over-threshold values.

The same dependences for two transverse field components are shown in Figures 5 and 6. The components b_ρ and b_ϕ for the magnetotail regions considered are nonzero, both parallel to the main current at the magnetopause and normal to it. For both transverse components, the coherence parameters for Both IN and the differences between the classes are smaller than for the longitudinal component. For b_ρ, there are almost no differences between MPCross and Both OUT, and their difference from Both IN is more pronounced in the probability of occurrence of over-threshold $\langle\gamma^2\rangle$ and γ^2_{max} than in the averages. For b_ϕ, the minimum coherence persists for MPCross, whereas Both IN and Both OUT differ little in coherence parameters. The differences between MPCross and the other two classes (as for b_ρ) are most clearly manifested in the probability of occurrence of over-threshold values.

Thus, the minimum coherence in the vicinity of the magnetopause, found in [Yagova, Evsina, 2024], exists for the transverse components for the entire range of interval lengths under study.

2.2. An example of coherent pulsation in the magnetosheath

In addition to the oscillations described in [Kim et al., 2002; Kepko et al., 2002] that directly penetrate into the magnetosphere from the interplanetary medium, pulsations “decoupled” from external fluctuations are recorded in the magnetosheath [Zastenker et al., 2002]. Yagova and Evsina [2024] have examined properties of such Pc5-6/Pi3 pulsations on both sides of the magnetopause. Below, the properties of long-period magnetic field pulsations are analyzed for the interval when both satellites were in the magnetosheath.

The pulsations occurred on June 22, 2016. Projections of satellite orbits and magnetospheric boundaries determined from [https://sscweb.gsfc.nasa.gov/] for the interval

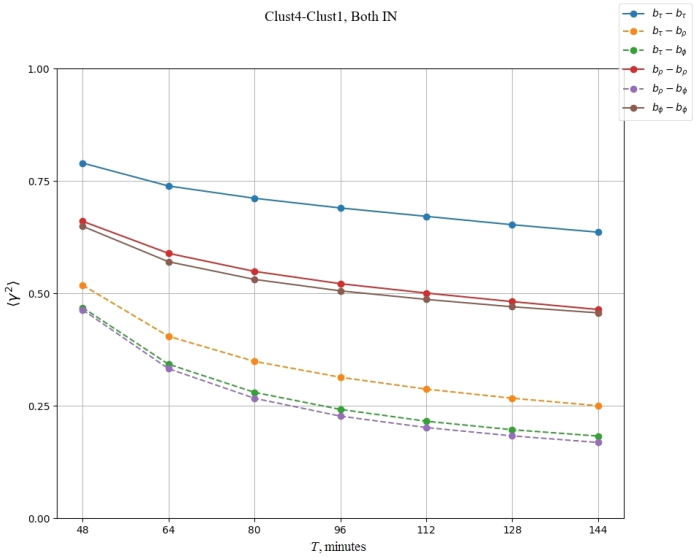

Figure 1. Dependences of band mean coherence $\langle\gamma^2\rangle$ on interval length T for longitudinal and transverse magnetic field components for satellites in tail lobes (Both IN): diagonal and nondiagonal elements are denoted by solid and dashed lines respectively

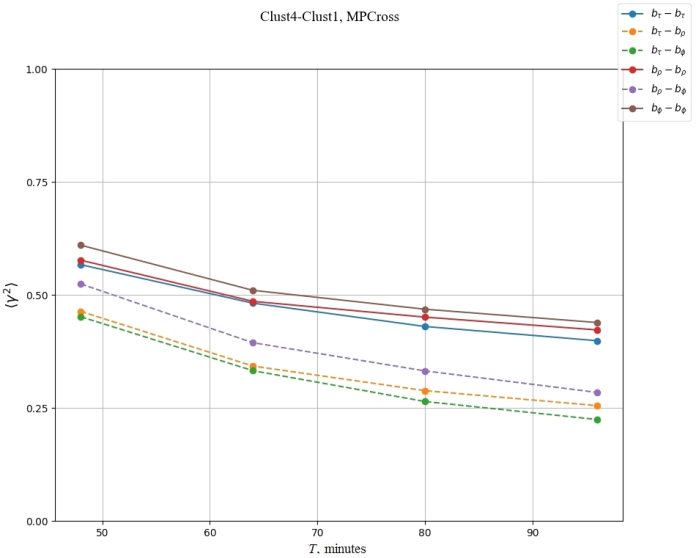

Figure 2. The same as in Figure 1 for the satellites in the vicinity of the magnetopause (MPCross)

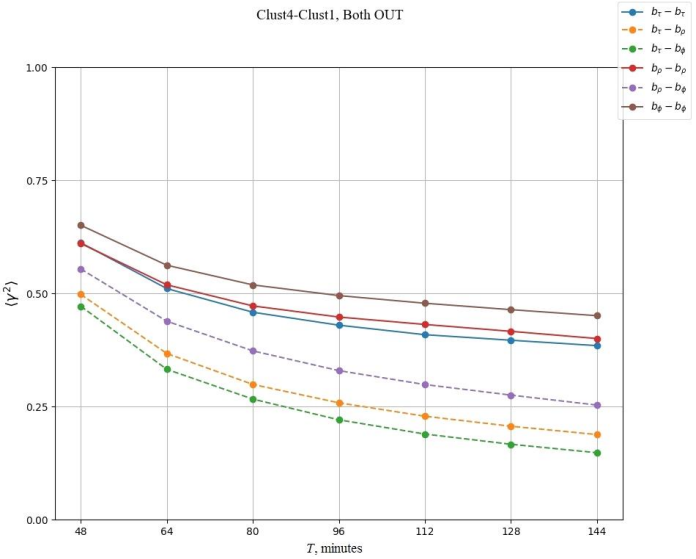

Figure 3. The same for the satellites in the flank magnetosheath (Both OUT)

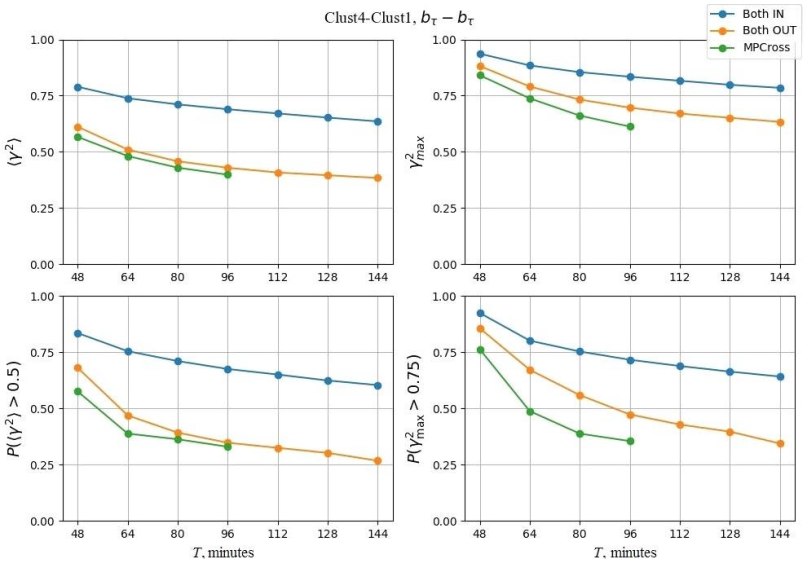

Figure 4. Coherence parameters versus interval length T for the longitudinal component b_τ: the average over all intervals of a given length (top panel) and the proportion of intervals with over-threshold coherence (bottom panel) for the band mean $\langle\gamma^2\rangle$ (left) and maximum γ^2_{max} (right)

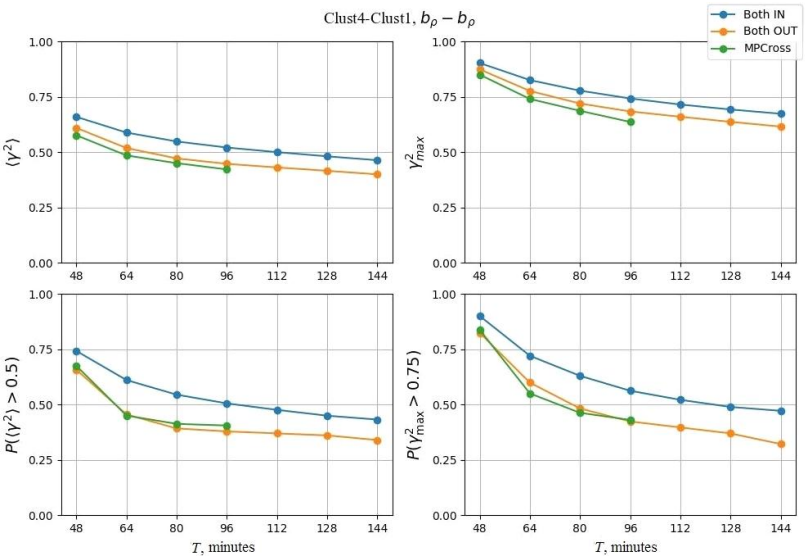

Figure 5. The same for the component b_ρ

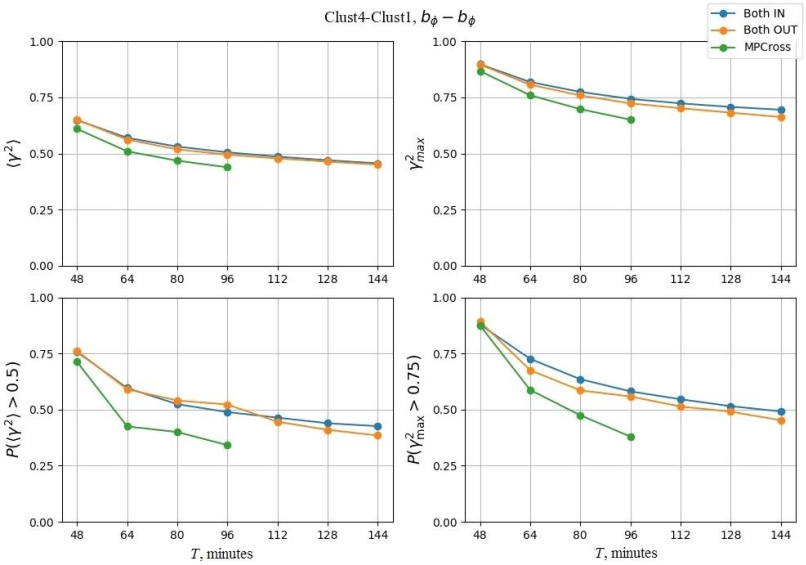

Figure 6. The same for the component b_ϕ

12:23–13:27 UT are depicted in Figure 7 together with the average IMF interval (recalculated to the subsolar point) and the magnetic field at the location of each of the Cluster satellites. Figure 7 uses the *X*–*R* projection, where $R^2=Y^2+Z^2$ of the GSE system. During the period considered, both satellites were in the near nightside magnetosheath, with the distance between the satellites being around $2R_E$, and Cluster-4 was closer to the subsolar point. The direction of the magnetic field at the positions of both satellites is almost normal to the magnetopause.

The PSD spectra for the three magnetic field components on the trajectory of each satellite are presented in Figure 8. In both cases, the main spectral power is concentrated in b_ϕ, and the main maximum is observed at f_1=1.5 mHz. Let us take a closer look into pulsations in b_ϕ. Figure 9 illustrates the time signal waveforms after high-pass filtration with a cutoff frequency of 0.8 mHz, the spectral coherence γ^2, and the phase difference $\Delta\phi$. The magnetograms (Figure 9, *a*) show a similarity between the waveforms and the phase incursion in the direction from Cluster-4 to Cluster-1, i.e. anti-sunward. The peak-to-peak amplitude is ~16 nT for Cluster-1 and 12 nT for Cluster-4, i.e. as they propagate, the amplitude increases.

The spectral coherence (Figure 9, *b*) reveals two maxima: the first at the frequency of the main spectral maximum $f_1\approx1.5$ mHz with $\gamma^2_{max}=0.75$, the second at the frequency $f_2=3.6$ mHz with a plateau in the power spectrum according to Cluster-4 data, whereas Cluster-1 data shows slowing of the decline in PSD with frequency. In the vicinity of f_1, the phase difference $\Delta\phi=140°$; and in the vicinity of f_2, $\Delta\phi\approx0$, i.e. the oscillations are nearly in phase.

Long-period pulsations in the magnetosheath can be either a response to quasi-periodic variations in IMF and P_{sw} in front of the bow shock, or they can form inside the "big magnetosphere" [Yagova, 2015]. To identify the nature of excitation of the observed oscillations, we examine variations in IMF components and P_{sw} in the same frequency range. Coherence time forms and spectra for P_{sw} and IMF components are displayed in Figure 10. Figure 10, *a*, *b* illustrates variations in P_{sw} and IMF B_y and B_z after high-pass filtration with the same cutoff frequency of 0.8 mHz as for magnetic field variations in the magnetosheath (lowercase letters are used for the variations to distinguish them from the complete value of the same variable). The peak-to-peak amplitude was ~2.5 nT for B_z and 1 nT for B_y, which is several times lower than that for b_ϕ in the magnetosheath, which exceeded 10 nT according to the data from both satellites (see Figure 9, *a*). The average peak-to-peak amplitude of P_{sw} was ~0.3 nPa; and the maximum, 0.5 nPa (Figure 10, *b*). This level of amplitudes is typical at low SW velocities. The spectral coherence of the variations both in P_{sw} (Figure 10, *c*) and in IMF components (Figure 10, *d*) with variations in b_ϕ in the magnetosheath does not exceed 0.3.

Let us now consider in more detail the conditions in the interplanetary medium for the time interval shown in Figures 7–10 and for 80 min before the interval. Figure 11 depicts variations in the three IMF components, SW velocity and dynamic pressure derived from OMNI data. The SW velocity $V\approx350$ km/s, and P_{sw} varied from 2.5 to 3 nPa. At around 11:40 UT, P_{sw} began to rise to 3.5 nPa simultaneously with a turn of B_z to the north during which its values changed from slightly negative to near-zero. Thus, there were no significant disturbances in the interplanetary medium either before or during the time interval considered. Against this background, quasi-periodic oscillations developed in the magnetosheath, coherent on scales of several R_E, which had predominantly transverse polarization and propagated anti-sunward.

3. DISCUSSION

Analysis of the dependence of coherence of long-period magnetic field variations on interval length *T* has revealed that differences in coherence values between pulsations in the magnetotail, in the vicinity of the magnetopause, and in the flank magnetosheath exist in the *T*

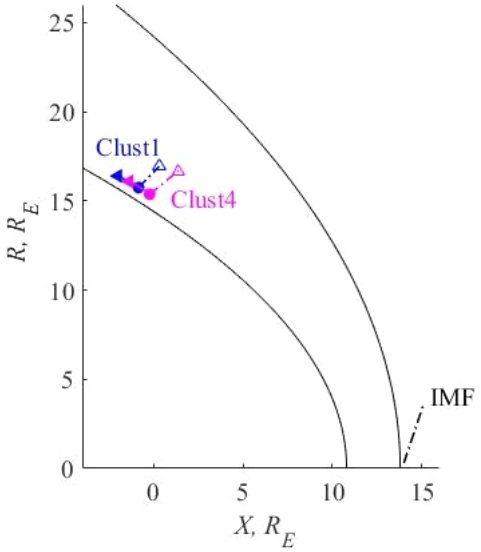

Figure 7. *X*–*R* projections of segments of satellites' orbits on June 22, 2016 (day 174) at 12:23–13:27 UT, magnetospheric boundaries according to [https://sscweb.gsfc.nasa.gov/], and interval-average magnetic field projection in front of the bow shock and in the magnetosheath. The direction of the satellite is indicated by an arrow; the direction of the magnetic field, by a dashed-dot line

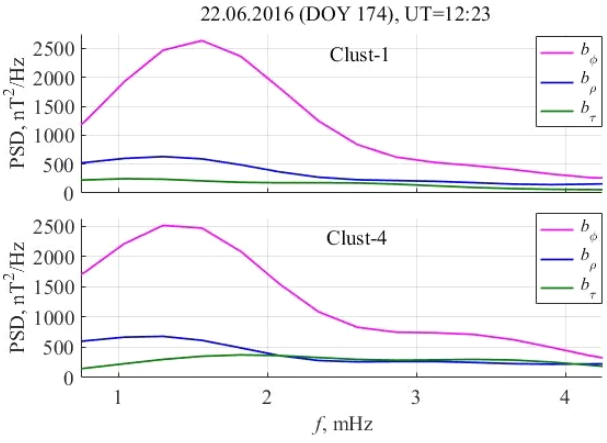

Figure 8. PSD spectra of magnetic field component variations for the interval 12:23–13:27 UT on June 22, 2016 (day 174) according to Cluster-1 and -4 data

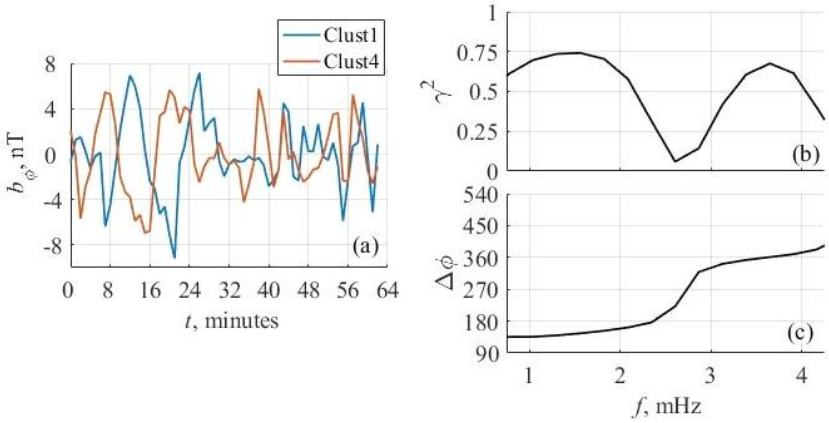

Figure 9. Magnetograms (*a*), spectral coherence γ^2 (*b*), and phase difference $\Delta\phi$ (*c*) of b_ϕ variations according to Cluster-1 and -4 data for the same time interval as in Figures 7, 8

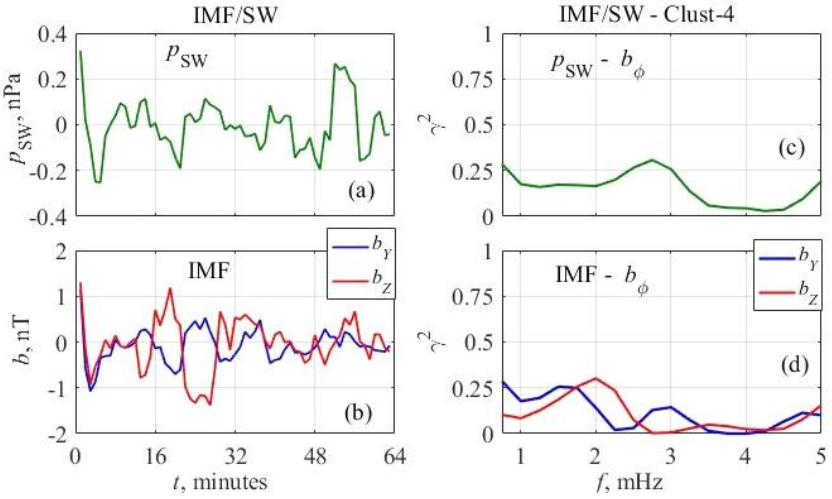

Figure 10. Filtered (f>0.8 mHz) variations of the SW dynamic pressure P_{sw} (*a*), the IMF B_y and B_z components (*b*), and their coherence with b_ϕ variations according to Cluster-4 data (*c*, *d*) for the same time interval

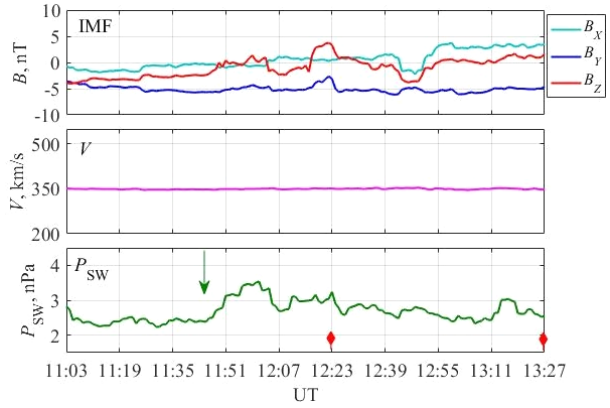

Figure 11. IMF components, SW velocity and dynamic pressure for the same time interval as in Figures 7–10 (highlighted in red) and for the preceding period. The arrow marks the beginning of P_{sw} increase

range from 48 min to ~2.5 hrs. Differences between coherence values for different satellite positions almost always increase with *T*.

These differences are most clearly manifested for variations in the longitudinal field component b_τ for which the maximum coherence is observed in the tail lobe (Both IN, τ-τ). It is for Both IN, τ-τ that coherence becomes maximum among all the explored combinations of magnetic field components and satellite positions.

Coherence in the tail lobe is lower for the transverse components than for the longitudinal one. For b_ϕ, values of the coherence parameters in the tail lobe and in the magnetosheath almost coincide in the entire *T* range, and their values are closer to those for Both OUT in the longitudinal component. The oscillations "decoupled" between positions of Both IN and Both OUT exist at least up to T=96 min, which is statistically manifested in lower coherence in the vicinity of the magnetopause. This confirms the conclusion drawn in [Yagova, Evsina, 2024] for one *T* and solar minimum.

For b_ρ, as well as for the longitudinal component b_τ, the maximum coherence is recorded in the tail lobe, but its numerical values are lower, as is the contrast of Both IN/Both OUT, which brings the picture closer to that observed for b_ϕ. The difference between Both OUT and MPCross for b_ρ is smaller than for the longitudinal component, and is virtually absent for the mean coherence.

A case study of coherent oscillations in the nightside magnetosheath has shown that their spectral composition

is formed inside the "big magnetosphere", they have the form of anti-sunward quasi-periodic variations with the 1.5 mHz frequency of the main maximum. The event develops at a low level of fluctuations in the interplanetary medium and a low SW velocity. Low coherence of magnetic variations in the magnetosheath and external fluctuations contradicts the conclusion drawn in [Gutynska et al., 2012] that in the low-frequency region the relationship with fluctuations in front of the bow shock is bound to manifest itself in low-frequency oscillations. This difference is probably due to the fact that in [Gutynska et al., 2012] the analysis was performed for the magnetic field modulus, ignoring transverse oscillations.

In almost the entire interval in question at the subsolar point, the ratio $|B_X|/|B_n|<0.5$, i.e. the conditions are closer to those for a quasi-perpendicular bow shock (B_n is the IMF component normal to the Sun–Earth line), whereas on the flank of the magnetopause the conditions are closer to those for a quasi-parallel bow shock. Accordingly, the source of the observed variations may be variations in the SW dynamic pressure on the transverse components of SW velocity and/or B_x variations, which are usually ignored [Belenkaya, 1998; Cowley, 1981; Kubyshkina et al., 2023]. Moreover, the high variability of plasma and magnetic field parameters requires us to analyze the actual distribution of the velocity field in the magnetosheath (see, e.g., [Shevyrev, Zastenker, 2005]), which is beyond the scope of this paper.

The properties of the time series under study may differ from those needed for correct application of standard statistical tests, and the mean coherence of quasi-periodic processes with a wide spectrum varies depending on their spectral content. Let us analyze the significance of the results. As an indicator of the relationship between the processes, we will use the excess of coherence for the data on the same time intervals of mean coherence for these data series at any given time. Compare the coherence values for the data from simultaneous measurements of the magnetic field and the same data with a nonzero displacement of one series relative to the other. Since we deal with the pulsations in the geomagnetic tail and in the magnetosheath, there are no diurnal variations in the pulsation parameters, and the time of t_s displacement is defined by two conditions. On the one hand, t_s should be longer than the interval length for which the spectral analysis was made, and on the other hand, the parameters outside the magnetosphere should not change too much during this period. From these requirements, we assume t_s=6 hr.

Figure 12 presents the band mean coherence for simultaneously measured and displaced data series for Both OUT intervals, the number of which is maximum at the same interval lengths as in Figures 1–6. For all pairs of components, the values of $\langle\gamma^2\rangle$ for displaced data are much lower than for simultaneous data. Thus, the test with displaced series indirectly confirms the significance of the results obtained.

The choice of the coordinate system for analyzing magnetic field variations in the presence of the boundary at which a discontinuity occurs in the direction of the main field is ambiguous. The adequacy of the chosen coordinate system is supported by higher values of the diagonal elements of the spectral coherence matrix than the nondiagonal ones (see Figures 1–3), and by the significant difference in the results between the longitudinal and transverse components (see Figures 4–6). Nevertheless, the choice of orientation of the transverse components, implemented according to the same scheme as in the inner magnetosphere, may not be optimal and requires verification for different satellite positions relative to the ecliptic plane and magnetospheric boundaries.

CONCLUSIONS

For all satellite positions relative to the magnetospheric boundaries and magnetic field components, the spectral coherence γ^2 decreases with interval length. For the lower limit of pulsation coherence $<\gamma_b^2>=0.5$, determined from the band mean γ^2, we have obtained the following main results.

Coherence is maximum for the longitudinal component of the magnetic field variations b_τ in the magnetotail lobe. For this component, pulsations in the magnetotail are coherent in the entire range of explored periods,

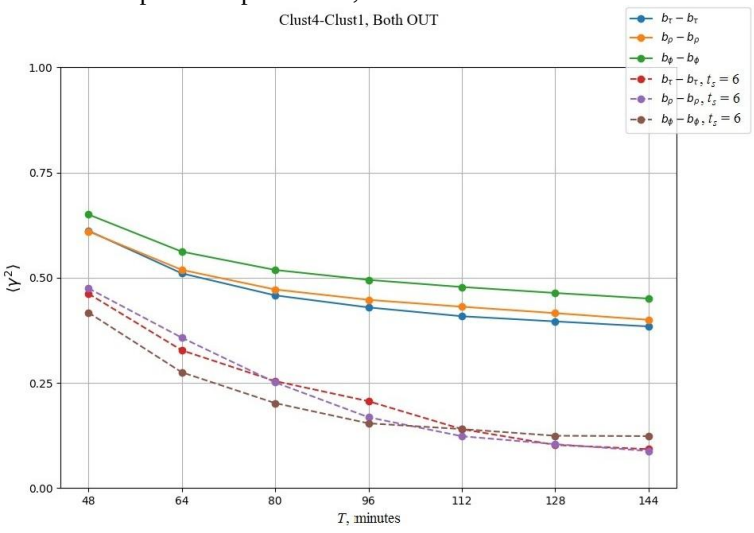

Figure 12. Dependences of band mean coherence $\langle\gamma^2\rangle$ on interval length T for magnetic field components and satellites' positions in the magnetosheath (Both OUT). The solid line denotes the dependences for simultaneous data; the dashed line, for displaced data

i.e. the coherence scale exceeds 2.5 hrs. For b_τ, the maximum contrast between the magnetotail and the magnetosheath is recorded: in the magnetosheath and in the vicinity of the magnetopause, the coherence scale is 1 hr.

For transverse components of magnetic field variations, the coherence scale varies from 1 hr to 100 min. The influence of the magnetopause is maximum for b_ϕ. For this component, the coherence scale is 100 min for the magnetotail and magnetosheath, and 1 hr for the vicinity of the magnetopause, which confirms the presence of Pc5/Pi3 pulsations in the flank magnetosheath, which are "decoupled" with both external fluctuations and pulsations in the tail.

For b_ρ, the coherence scale is 100 min for the magnetotail, as for b_ϕ; and 1 hr for the magnetosheath and the vicinity of the magnetopause, as for b_τ.

Quasi-harmonic transverse ULF wave disturbances, coherent in the magnetosheath and "decoupled" from external fluctuations, can develop at low SW velocities and intensity of IMF and SW dynamic pressure fluctuations.

We are grateful to the reviewers for their careful reading of the manuscript and helpful comments. For the analysis, we used measurement data on the magnetic field from the Cluster satellites and on IMF and SW parameters from [https://cdaweb.gsfc.nasa.gov/cgi-bin/eval2.cgi].

The work was financially supported by the Russian Foundation for Basic Research (Project No. 24-77-10012).

REFERENCES

Alexandrova O., Lacombe C., Mangeney A. Spectra and anisotropy of magnetic fluctuations in the Earth's magnetosheath: Cluster observations. *Ann. Geophys.* 2008, vol. 26, pp. 3585–3596. DOI: 10.5194/angeo-26-3585-2008.

Belenkaya E.S. Reconnection modes for near-radial interplanetary magnetic field. *J. Geophys. Res.* 1998, vol. 103, pp. 26487–26494. DOI: 10.1029/98JA02270.

Cowley S.W.H. Asymmetry effects associated with the x-component of the IMF in a magnetically open magnetosphere. *Planet. Space Sci*. 1981, vol. 29, iss. 8, pp. 809–818. DOI: 10.1016/0032-0633(81)90071-4.

Escoubet C.P., Fehringer M., Goldstein M. The Cluster mission. *Ann. Geophys.* 2001, vol. 19, pp. 1197–1200. DOI: 10.5194/angeo-19-1197-2001.

Escoubet C.P., Masson A., Laakso H., Goldstein M.L. Recent highlights from Cluster, the first 3-D magnetospheric mission. *Ann. Geophys*. 2015, vol. 33, pp. 1221–1235. DOI: 10.5194/angeo-33-1221-2015.

Gutynska O., Šafránková J., Němeček Z. Correlation length of magnetosheath fluctuations: Cluster statistics. *Ann. Geophys*. 2008, vol. 26, pp. 2503–2513. DOI: 10.5194/angeo_26_2503_2008.

Gutynska O., Šafránková J., Němeček Z. Correlation properties of magnetosheath magnetic field fluctuations. *J. Geophys. Res*. 2009, vol. 114, no. A8, A08207. DOI: 10.1029/2009JA014173.

Gutynska O., Šimůnek J., Šafránková J., et al.. Multipoint study of magnetosheath magnetic field fluctuations and their relation to the foreshock. *J. Geophys. Res*. 2012, vol. 117, A04214. DOI: 10.1029/2011JA017240.

Huang S.Y., Hadid L.Z., Sahraoui F., et al. On the existence of the Kolmogorov inertial range in the terrestrial magnetosheath turbulence. *Astrophys. J. Lett.* 2017, vol. 836, L10. DOI: 10.3847/2041-8213/836/1/L10.

Kepko L., Spence H.E., Singer H.J. ULF waves in the solar wind as direct drivers of magnetospheric pulsations. *Geophys. Res. Lett.* 2002, vol. 29, iss. 8. DOI: 10.1029/2001GL014405.

Kim K.-H., Cattell C.A., Lee D.-H., et al. Magnetospheric responses to sudden and quasiperiodic solar wind variations. *J. Geophys. Res*. 2002. vol. 107, iss. A11, p. 1406. DOI: 10.1029/2002JA009342.

Kubyshkina M.V., Semenov V.S., Tsyganenko N.A., et al. Unraveling the role of IMF B_x in driving geomagnetic activity. *J. Geophys. Res.: Space Phys*. 2023, vol. 128, e2022JA031275. DOI: 10.1029/2022JA031275.

Leonovich A.S., Mazur V.A., Kozlov D.A. MHD waves in the geomagnetic tail: A review. *Sol.-Terr. Phys*. 2015, vol. 1, iss. 1, pp. 4–22. DOI: 10.12737/7168.

Nosikova N.S., Yagova N.V., Baddeley L.J., et al. An investigation into the spectral parameters of ultra-low-frequency (ULF) waves in the polar caps and magnetotail. *Ann. Geophys*. 2022, vol. 40, pp. 151–165. DOI: 10.5194/angeo-40-151-2022.

Rakhmanova L., Riazantseva M., Zastenker G., Yermolaev Y. Dynamics of plasma turbulence at Earth's bow shock and through the magnetosheath. *Astrophys. J*. 2020, vol. 901, p. 30. DOI: 10.3847/1538-4357/abae00.

Rakhmanova L., Riazantseva M., Zastenker G., Yermolaev Y. Role of the variable solar wind in the dynamics of small-scale magnetosheath structures. *Frontiers in Astronomy and Space Sciences*. 2023, vol. 10. DOI: 10.3389/fspas.2023.1121230.

Rakhmanova R., Khokhlachev A., Riazantseva M., et al. Turbulence development behind the bow shock during disturbed and undisturbed solar wind. *Sol.-Terr. Phys.* 2024, vol. 10, no. 2, pp. 13–25. DOI: 10.12737/stp-102202402.

Shevyrev N.N., Zastenker G.N. Some features of the plasma flow in the magnetosheath behind quasi-parallel and quasi-perpendicular bow shocks. *Planet. Space Sci*. 2005, vol. 53, pp. 95–102. DOI: 10.1016/j.pss.2004.09.033.

Shevyrev N.N., Zastenker G.N., Nozdrachev M.N., et al. High and low frequency large amplitude variations of plasma and magnetic field in the magnetosheath: Radial profile and some features. *Adv. Space Res.* 2003, vol. 31, pp. 1389–1394. DOI: 10.1016/S0273-1177(03)00008-5.

Shevyrev N.N., Zastenker G.N., Du J. Statistics of low-frequency variations in solar wind, foreshock and magnetosheath: INTERBALL-1 and CLUSTER data. *Planetary Space Sci*. 2007, vol. 55, pp. 2330–2335. DOI: 10.1016/j.pss.2007.05.014.

Stukov D.A., Yagova N.V. Coherence time scales of magnetic field pulsations in 1–5 mHz range in the magnetotail and night magnetosheath. Proc. Baikal Young Scientists' International School On Fundamental Physics (BASYS-2024) "Physical Processes in Outer and Near-Earth Space" and XVIII Young Scientists' Conference "Interaction of Fields and Radiation with Matter"]. Irkutsk, September 1–7, 2024. Institute of Solar-Terrestrial Physics, Irkutsk, 2024, pp. 220–222. (In Russian).

Wang G.Q., Zhang T.L., Ge Y.S. Spatial distribution of magnetic fluctuation power with period 40 to 600 s in the magnetosphere observed by THEMIS. *J. Geophys. Res.: Space Phys*. 2015, vol. 120, pp. 9281–9293. DOI: 10.1002/2015JA021584.

Yagova N.V. Spectral slope of high-latitude geomagnetic disturbances in the frequency range 1–5 mHz. Control parameters inside and outside the magnetosphere. *Geomagnetism and Aeronomy*. 2015, vol. 55, pp. 32–40. DOI: 10.1134/S0016793215010144.

Yagova N.V., Evsina N.S. Geomagnetic pulsations in the 1–4 mHz frequency range (Pc5/Pi3) in the magnetotail. Internal and extramagnetospheric sources. *Cosmic Res*. 2024, vol. 62, no. 4, pp. 323–329. DOI: 10.1134/S0010952524600355.

Yagova N.V., Kozyreva O.V., Nosikova N.S. Geomagnetic pulsations in 1–4 mHz frequency range (Pc5/Pi3) in the magnetotail at different levels of disturbances in the interplanetary medium. *Sol.-Terr. Phys*. 2022, vol. 8, iss. 3, pp. 76–83. DOI: 10.12737/stp-82202212.

Zastenker G.N., Nozdrachev M.N., Němeček Z., et al. Multispacecraft measurements of plasma and magnetic field variations in the magnetosheath: Comparison with Spreiter models and motion of the structures. *Planetary Space Sci*. 2002, vol. 50, iss. 5-6, pp. 601–612. DOI: 10.1016/S0032-0633(02)00039-9.

URL: https://cdaweb.gsfc.nasa.gov/ (accessed March 31, 2025).

URL: https://cdaweb.gsfc.nasa.gov/cgi-bin/eval2.cgi (accessed March 31, 2025).

The paper is based on material presented at the 20th Annual Conference on Plasma Physics in the Solar System, February 10–14, 2025, Space Research Institute RAS, Moscow, Russia.

Original Russian version: Stukov D.A., Yagova N.V., published in Solnechno-zemnaya fizika. 2025, vol. 11, no. 4, pp. 132–142. DOI: 10.12737/szf-114202513.

How to cite this article

Stukov D.A., Yagova N.V. Coherence time scales of long-period ULF variations of magnetic field in vicinity of the night-side magnetopause. *Sol.-Terr. Phys*. 2025, vol. 11, iss. 4, pp. 120–129. DOI: 10.12737/stp-114202513.